

Graphical Abstract

A Fully Automated DM–BIM–BEM Pipeline Enabling Graph-Based Intelligence, Interoperability, and Performance-Driven Early Design

Jun Xiao, Qiong Wang, Yihui Li, Zhexuan Yu, Hao Zhou, Borong Lin

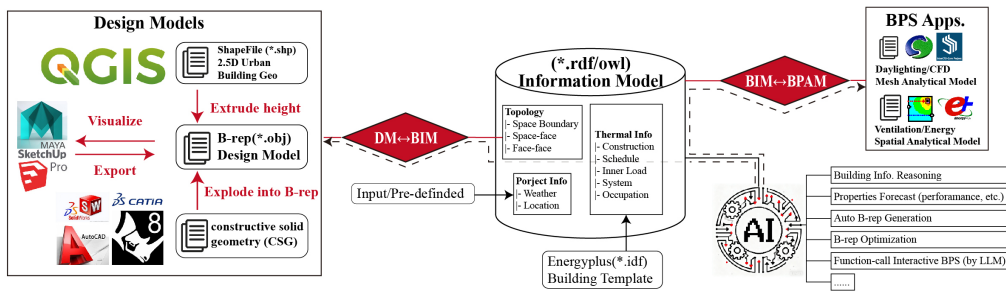


Figure 1: Potential applications with this framework.

Highlights

A Fully Automated DM–BIM–BEM Pipeline Enabling Graph-Based Intelligence, Interoperability, and Performance-Driven Early Design

Jun Xiao, Qiong Wang, Yihui Li, Zhexuan Yu, Hao Zhou, Borong Lin

- Automated DM–BIM–BEM transformation for AI-enabled early design
- Knowledge-graph topology linking geometry, spaces, and performance data
- High fidelity topology extraction for early-stage building analysis
- Extends BIM- and KG-based AI workflows to flexible B-rep design models
- Expands usable data for learning-based design and construction automation

A Fully Automated DM–BIM–BEM Pipeline Enabling Graph-Based Intelligence, Interoperability, and Performance-Driven Early Design

Jun Xiao^{a,b}, Qiong Wang^a, Yihui Li^a, Zhexuan Yu^a, Hao Zhou^{b,c}, Borong Lin^{a,b,*}

^a*Department of Building Science, School of Architecture, Tsinghua University, Beijing, 100084, Beijing, China*

^b*Key Laboratory of Eco Planning & Green Building, Ministry of Education, Tsinghua University, Beijing, 100084, Beijing, China*

^c*Institute for Urban Governance and Sustainable Development, Tsinghua University, Beijing, 100084, Beijing, China*

Abstract

Artificial intelligence in construction increasingly depends on structured representations such as Building Information Models and knowledge graphs, yet early-stage building designs are predominantly created as flexible boundary-representation (B-rep) models that lack explicit spatial, semantic, and performance structure. This paper presents a robust, fully automated framework that transforms unstructured B-rep geometry into knowledge-graph-based Building Information Models and further into executable Building Energy Models. The framework enables artificial intelligence to explicitly interpret building elements, spatial topology, and their associated thermal and performance attributes. It integrates automated geometry cleansing, multiple auto space-generation strategies, graph-based extraction of space and element topology, ontology-aligned knowledge modeling, and reversible transformation between ontology-based BIM and EnergyPlus energy models. Validation on parametric, sketch-based, and real-world building datasets demonstrates high robustness, consistent topological reconstruction, and reliable performance-model generation. By bridging design models, BIM, and BEM, the framework provides an AI-oriented infrastructure that extends BIM- and graph-based intelligence pipelines to flexible early-stage design geometry, en-

*Corresponding author. E-mail: linbr@tsinghua.edu.cn

abling performance-driven design exploration and optimization by learning-based methods.

Keywords:

Model Transformation, B-rep Model, Knowledge Graph, Building Information Model, Building Energy Model

1. Introduction

Most high-impact design decisions governing building performance are made during the early design stage; it is estimated that more than 40% of potential energy savings are determined at this phase [1]. As a result, architects and designers increasingly seek computational support that can operate directly on early-stage design representations, accommodate rapid iteration, and provide actionable feedback without imposing heavy modeling overheads [2]. This demand has driven growing interest in artificial intelligence (AI) techniques—such as graph neural networks (GNNs), large language models (LLMs), and knowledge-based reasoning—to augment early design decision-making.

Despite their promise, AI-driven design workflows remain constrained by a representation gap between early-stage design data and the forms of abstraction required for effective reasoning. While recent AI models can extract geometric features from images, meshes, or voxelized representations, these encodings primarily capture low-level spatial occupancy or visual patterns and do not explicitly represent higher-order spatial hierarchies, element adjacencies, or functional relationships[3]. As a result, their capacity for relational inference, semantic interpretation, and performance-aware reasoning remains limited. In contrast, AI models that reason over spatial configuration, element relationships, and performance-relevant attributes benefit from graph-based encodings—such as Knowledge Graphs (KGs) or Network Graphs (NGs)—which provide explicit structure, relational context, and semantic grounding. Building Information Models (BIM), particularly when encoded as ontology-based KGs, offer a well-suited abstraction layer for such AI interpretation by explicitly representing spaces, elements, their topological relationships, and associated physical or operational attributes.

Recent research has demonstrated the potential of KG- and NG-based AI in the built environment, supporting applications such as semantic reasoning, language-based model interrogation, automated design recommenda-

tions, and performance prediction [4, 5]. NG representations further enable data-driven learning via GNNs, including building- and neighborhood-scale performance estimation [6]. However, these advances remain largely confined to well-structured BIM datasets, whereas the vast majority of early design models—and most practically available design data—exist as unstructured B-rep geometries without explicit spatial topology or semantic annotation. This mismatch severely limits the applicability and scalability of AI in early-stage design.

From a transformation perspective, enabling AI intervention for performance-driven design requires two tightly coupled and reversible processes: (1) converting unstructured design models into structured, graph-based BIM representations suitable for AI interpretation, and (2) extending these BIMs into analytical models that encode performance-related attributes, allowing AI to reason about, predict, or optimize building behavior. These processes correspond to transformations between three distinct model types with fundamentally different representational intents:

Design Models (DM) capture only the geometric configuration of buildings, typically using boundary-representation (B-rep) schemas (faces, edges, normals, materials) as in SketchUp or Autodesk Maya, or Constructive Solid Geometry (CSG) using volumetric primitives. Early-stage DMs intentionally remain minimal—lacking semantic structure or thermal attributes—to maximize flexibility during conceptual design.

Building Information Models (BIM) formalize spatial hierarchies, element attributes, and semantic relationships. They are frequently encoded in the Web Ontology Language (OWL) through domain ontologies such as BOT [7] or BRICK [8], with the IFC schema (*.ifc) and its ifcOWL representation [9] serving as the dominant standard. These OWL-based BIMs can be represented as Knowledge Graphs (KGs) consisting of RDF triplets, or equivalently as Network Graphs (NGs) of nodes and edges.

BPS Analytical Models (BPAM) extend BIM by embedding simulation-specific parameters into spaces and building elements. Required information varies by engine: space–face–space topology for multi-zone energy or airflow analysis, system topology for system-dynamics tools (e.g., TRNSYS, VENSIM), and categorized meshes or volumetric partitions for daylighting or CFD. This work focuses on the Building Energy Model (BEM), the most information-intensive form of BPAM.

The major obstacle to AI-enabled automation lies in the DM-to-BIM transformation. Converting a B-rep model into a graph-based BIM requires

recovering spatial hierarchies and computing explicit topology, most critically the space–face relationships defined as the 1st Level Space Boundary (1LSB)[10] and the face–face adjacencies defined as the 2nd Level Space Boundary (2LSB) [11]. Existing methods predominantly focus on 2LSB extraction within structured IFC models (Table 1), implicitly assuming that spaces are already defined. This assumption breaks down entirely for early-stage B-rep models, where spaces are implicit and must be inferred. Auto Space Generation (ASG), corresponding to 1LSB computation, remains insufficiently addressed, with existing approaches relying on idealized geometries, limited layouts, or narrowly constrained input formats.

The transformation between BIM and BEM introduces additional challenges. OWL-based BIMs must be translated into analytical representations by associating elements and spaces with performance-related parameters. Prior studies have explored transformations to EnergyPlus or Modelica, often focusing on validation of OWL models [12] or template-based population of missing attributes [13]. While effective in controlled settings, such approaches are inflexible and poorly suited to AI-driven workflows, where models must be generated, modified, and evaluated automatically and at scale. Moreover, inconsistencies between ontologies, file formats, and simulation requirements further fragment the transformation pipeline, undermining interoperability and automation (Table 2).

As a result, current methods do not yet provide a stable, fully automated infrastructure that bridges unstructured design geometry, graph-based BIM representations, and performance-aware analytical models in a way that is compatible with AI workflows. In particular, no unified framework exists that (i) robustly derives spatial and element topology from heterogeneous B-rep inputs, (ii) encodes this information as KG- or NG-based BIM suitable for AI reasoning, and (iii) connects these representations to performance models that enable learning-based evaluation and optimization. To address these gaps, this article introduces a comprehensive DM→BIM→BEM transformation framework with the following contributions:

Fully automated and reversible transformation. The framework performs end-to-end automated conversion—from DM to OWL-based BIM and finally to a BEM in EnergyPlus (*.idf)—with each stage reversible and each module interchangeable, enabling plug-and-play integration of state-of-the-art algorithms. All materials and code are released openly.

Broad format support with ontology-consistent alignment. To ensure data coherence across transformations, the framework accepts multi-

ple common B-rep formats (*.obj, *.stl, etc.) and generates an intermediate OWL model aligned with major ontologies (ifc4.0, gbXML, BOT, WGS, etc.), enabling seamless downstream conversion through existing ontology-alignment modules.

Quantified validation on diverse datasets. Accuracy, robustness, and computational performance have been evaluated against comparable software using three datasets: 100 procedurally generated B-rep models, 570 manually created models from architecture students, and 15 complex real-building cases, with all metrics systematically assessed.

Through these contributions, the proposed framework repositions DM, BIM, and BEM not as isolated deliverables, but as interoperable, graph-based information infrastructures that enable scalable automation and AI intervention across early-stage building design and construction workflows. By providing a reliable transformation from unstructured design geometry to topology-aware knowledge graphs and performance-ready analytical models, the framework removes a critical bottleneck that has long limited the deployment of AI in construction informatics. It enables automated reasoning, learning, and optimization to operate directly on conceptual design data, supporting applications such as graph-based prediction, knowledge-driven design assistance, and performance-informed decision-making. In doing so, the framework advances the integration of design modeling, information management, and performance analysis into a unified, machine-interpretable pipeline, contributing a foundational automation layer for next-generation digital construction workflows.

2. Method

The workflow of the framework is generally serialized in two transformation tasks divided into eight modules (Fig.2).

2.1. Design Model to Building Information Model Transformation

This transformation provides a module that converts a design-oriented, stream-based B-rep file (.geo) into an Information Graph file (.owl or *.gbxml). The framework interfaces with widely used B-rep formats through a translation module for *.stl and *.obj files, and automatically performs geometric cleansing during the conversion process.

Table 1: Input Requirements and Corresponding Outputs of Relevant Studies

Ref.	Input Requirement	Output		
	Element & Geometries	Efficiency	1LSB	2LSB
[14]	No gaps and clashes Classified Elements	3.39s/space	N/A	Face-Space topology (IFC2x3)
[15]	No gaps and clashes Classified Elements	N/A	N/A	Face-Face topology Face-Space topology
[16]	No gaps and clashes Classified Elements	0.10s/Space	N/A	Face-Face topology Face-Space topology (IFC4)
[17]	No gaps and clashes Classified Elements	7.19s/Space	N/A	Face-Face topology Face-Space topology (IFC4)
[18]	no gaps and clashes fully aligned floors and walls Closed loop of walls	0.17s/Space	3d-1LSB	Face-Space topology
[19]	Geometry with minimal gaps only space boundary element	3.10s/Space	3d-1LSB	Face-Space topology
[20]	No gaps and clashes Closed loop of walls	0.06s/Space	3d-1LSB	Face-Space topology

Table 2: Input Requirements and Simulation Targets of Relevant Studies

Ref.	Input Requirement	Ontology	Sim. format	Sim. target
[13]	1LSB/2LSB Geometry Semantic information	PGD, BRICK, BOT	EnergyPlus	Sketch stage BPS
[21]	2LSB Geometry HVAC system topology Material properties	IFC4, Brick Schema	EnergyPlus	Indoor temperature energy consumption
[22]	2LSB HVAC system topology Material properties	IFC, IDS, Labelled Property Graph (LPG)	Modelica BuildSys, AixLib libraries	Dynamic energy assessment, baseline and renovation scenario evaluation
[23]	2LSB Geometry Material properties Occupancy scenarios	IFC4, gbXML	Modelica BuildSysPro library (Dymola)	Building energy model digital twins, energy assessment
[24]	2LSB Geometry HVAC system topology Material properties	IFC, MVD	Modelica (AixLib, HKESim), EnergyPlus, CFD	BEPS HVAC simulation, CFD, Life Cycle Assessment (LCA)
[25]	IFC4 with IDEAS library	IDM, MVD	Modelica	building with Modelica Library
[26]	2LSB Geometry HVAC system topology Material properties Occupancy scenarios	IFC4, IDM, MVD	EnergyPlus Modelica (AixLib, BuildSys)	Generic energy simulation

2.1.1. Face Classification

The face classification operates based on face attributes, transparency, and normals. In this framework, faces must be categorized into at least four classes for subsequent processing: walls, planes, glazing, and skylights. This classification accelerates the geometric cleansing process by reducing the number of Boolean operations required. In addition, topology computation also relies on basic face classification [18]. After filtering out faces that do not contribute to the spatial structure, the process produces more detailed face tags (e.g., shading, extra content, internal mass, etc.) for use in later stages of the workflow.

2.1.2. Cleanse

The cleansing process is a critical component for ensuring the robustness of the transformation. In this framework, the data-cleansing procedure comprises six primary sub-modules (Fig. 3):

`solve_duplicated` (Optional): Identifies and removes faces with identical levels, 2D projections, and heights. Faces are considered duplicates when their 2D projections coincide and all coordinates fall within a prescribed threshold.

`solve_redundant` (Optional): Detects and merges co-planar faces. This step is essential for mesh-based inputs (e.g., `*.stl`). An edge dictionary is

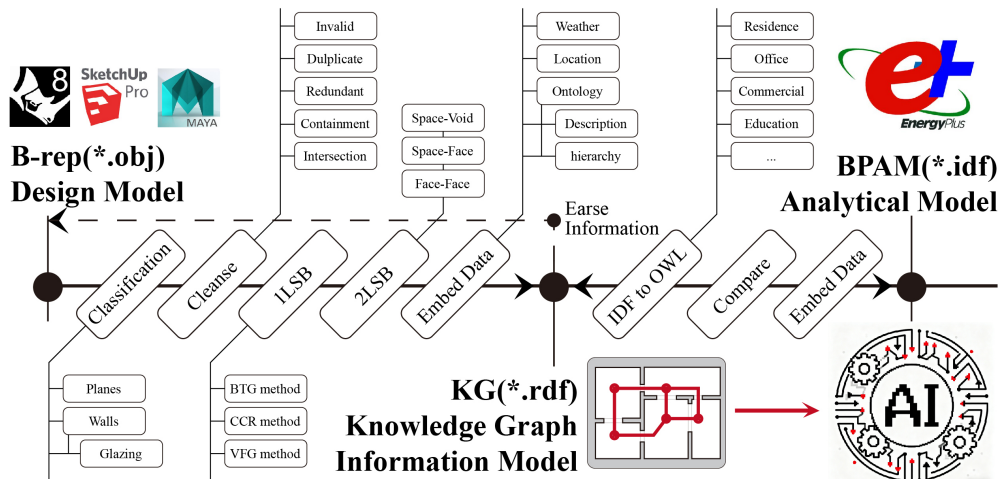


Figure 2: Modules in the transformation framework. Each module is a stand-alone method and allows substitution following the API documentation on the project

constructed to identify shared edges, allowing faces with identical normals to be merged.

`solve_containment` (Optional): Identifies overlapping or enclosed co-planar faces. Containment is detected when faces on the same level have intersecting 2D projections.

`solve_invalid`: Removes invalid faces, including those with degenerate projections, self-intersections, or incorrect geometric dimensions.

`break_wall_vertical` (Optional): Splits walls spanning multiple building levels to support multi-level thermal zone identification. Walls with vertical extents exceeding two levels are segmented.

`break_wall_horizontal` (Optional): Subdivides walls at their intersections with other walls. This is required for B-rep models lacking precomputed face intersections, ensuring proper segmentation of vertical faces.

2.1.3. First-Level Space Boundaries (1LSBs) Generation

The 1LSBs define the envelope surfaces of a space in a fusiform structure [27], consisting of a floor (potentially composed of multiple planes), a roof (also with multiple planes), and a 2D boundary formed by a closed loop of walls. Three representative Auto Space Generation (ASG) methods capable of computing 1LSBs have been reproduced, optimized, and integrated into this framework (Fig. 4).

The Building Topology Graph (BTG) method [18] constructs fusiform structures directly from face-face connectivity. It has been applied in Sefaira (Sefaira 2023) for SketchUp DM transformation. Although computationally efficient, BTG struggles with complex geometries such as vertically curved walls (walls composed of multiple vertical faces) or atria extending across multiple storeys.

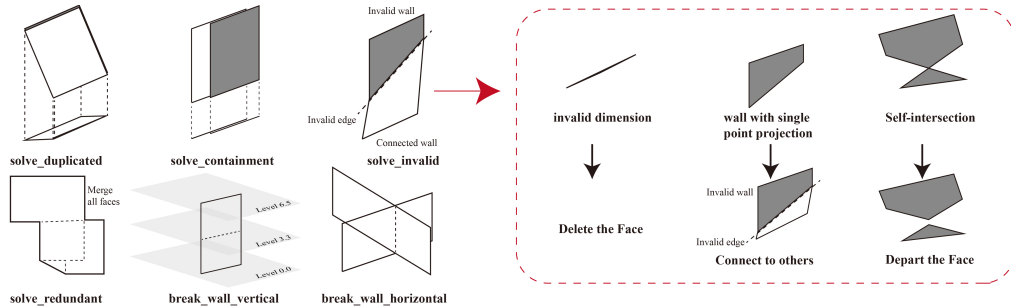


Figure 3: visualization of 6 cleansing methods

The Close Contour Recognition (CCR) method [20] identifies 2D 1LSBs using a dimension-reduced model in which faces are assigned to storeys, and then generates 3D 1LSBs through Boolean operations between 2D boundaries and planes. This approach, similar to AutoCAD's hatch-area identification, is computationally more intensive but offers greater robustness for storey-based architectural designs.

The View Factor Graph (VFG) method [19] computes visibility between surfaces to assemble closed fusiform spaces. It requires substantial ray–mesh Boolean computation but allows accuracy–efficiency trade-offs by adjusting ray density. Moreover, it remains robust when edge gaps between faces are smaller than the ray solid angle.

2.1.4. Second-Level Space Boundaries (2LSBs) Generation

This stage extracts the topological relationships between identified thermal zones and their bounding insulation elements (2LSB), thereby forming a complete multi-zone space network. The 2LSB definitions follow the IFC 4.x ontology [11]. Any 2LSB computation method can be integrated into the framework, provided it adheres to the class definitions of elements (WALL, FACE, GLAZING, SKYLIGHT) and spaces (SPACE, VOID).

Numerous mature 2LSB generation approaches exist (Table. 1). In this framework, a graph-based method is adopted. Building upon the 1LSB results, containment relationships between SPACE and VOID entities, as well as adjacency between VOID entities, are evaluated. This enables flexible rep-

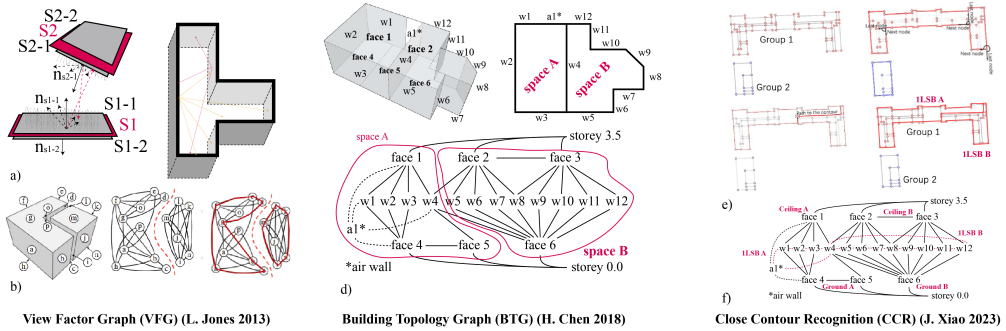


Figure 4: ASG methods description. a) The view factors to link elements, each element has 2 surfaces; b) Split the connection network on elements and calculate the envelope; c) The topology and space relations to identify by BTG; d) The fusiform structure of two spaces; e) The recursively division logic of the CCR method; f) Boolean and location of the ceilings and grounds.

resentation of complex geometries: for example, an atrium can be modelled as multiple vertically connected VOID entities bounded by a floor and ceiling, while a courtyard is represented as one or more VOID entities without an upper boundary.

Once the space-face associations are established, identifying space-space connectivity becomes straightforward, leading to the derivation of 2LSB relationships. The orientation factor for 2LSB is determined by evaluating the clockwise direction of each 2D 1LSB boundary. The final output is a connected thermal-zone network as illustrated in Fig. 5.

To align the data requirement of the Ontologies, especially the Building Topology Ontology (BOT)[7] to record space information, the 1LSB and 2LSB data should be restructured hierarchically into the series of Model-Building-Storey-Zone-Element-Sub element. Besides, the 2LSB relations and the geometry vertices information are integrated into the structure as KG.

2.2. Building Information Model to Building Energy Model Transformation

Given the limited thermal information typically available in early-stage design models, external boundary conditions and thermal settings must be imported and integrated into the OWL model. To ensure consistent alignment of space topology, geometry, and thermal properties, several established ontologies are adopted as the foundation of the proposed model (Fig. 6).

The ontology extends the KG-based BEM transformation schema (PGD) [13] and incorporates geometry information from WGS and GEO [28], as

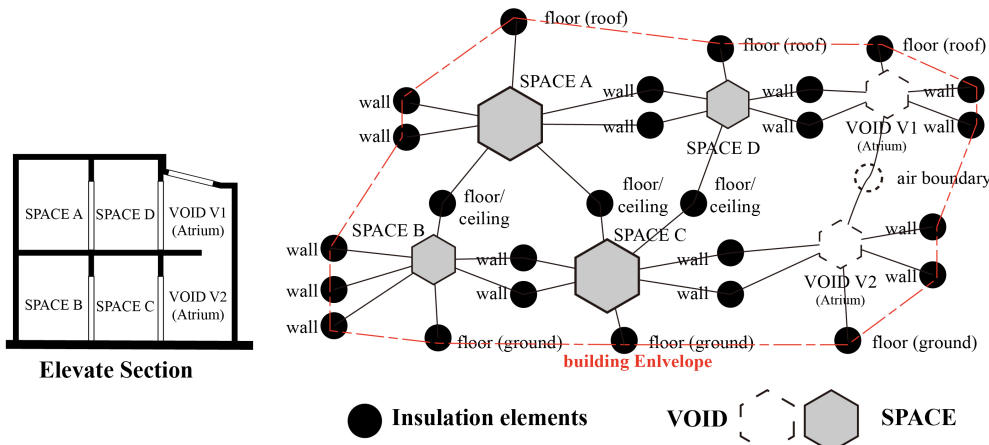


Figure 5: space network as a graph composed by SPACE and VOID

well as 1LSB and 2LSB definitions from IFC 4.0 [9], providing interoperability with CAD and IFC-based BIM. Basic HVAC and internal-gain concepts are integrated through the Brick Schema [8], while building topology follows the BOT ontology [7]. Components not covered by these existing ontologies (Brick, BOT, IFC4.0, WGS, PGD) are defined with the mos prefix for modularity and reproducibility.

The framework supports full export and import of KG-based model files (*.ttl, *.owl, *.xml). An additional alignment module enables export to *.gbXML, though *.gbXML import is not supported. Existing alignment tools (ifcOWL, Brick, DERIROOMS, etc.) can also be applied. However, due to the incomplete thermal data characteristic of early design, the alignment workflow by Wu et al.[13] is not adopted; instead, a more flexible transformation method tailored to early-stage models is implemented.

Following existing transformation workflows, a bidirectional conversion module between OWL and EnergyPlus *.idf is developed (Fig. 7). Users may attach an *.idf template containing HVAC, construction, schedule, and activity parameters, which are then adapted and embedded into the KG model (Fig. 7). During template processing, geometry and topology in the template file are ignored; only zone-level thermal attributes (HVAC, ventilation, internal gains) are preserved and mapped to all valid spaces derived from the B-rep model.

To ensure EnergyPlus compatibility, a standardization module is included. If BEM export is required, all vertical faces are reconstructed using the bottom-top 2D 1LSB projections, forming closed loops that guarantee full connectivity with floors and ceilings. This strictly satisfies EnergyPlus geometric constraints and preserves radiative heat-transfer accuracy. Users may opt to skip this reconstruction; in that case, EnergyPlus automatically falls back to a simplified solar distribution mode (FullExterior instead of FullInteriorAndExterior).

2.3. Validation

This article introduces a large mixture B-rep model dataset (Fig. 8) to evaluate and refine the developed module. Comprehensive building models including 200 parametric models (dataset 1), 570 sketch design models (dataset 2), and 15 complex real-building models (dataset 3) was curated, for the validation on the topology accuracy, analytical model accuracy, robustness, the and the efficiency in different applications.

A series of parametric models (dataset 1) are created by an auto-mass-generation module Evomass [29] for the sake of derivable space topology and accurate *.idf modelling. The grasshopper module Evomass can create

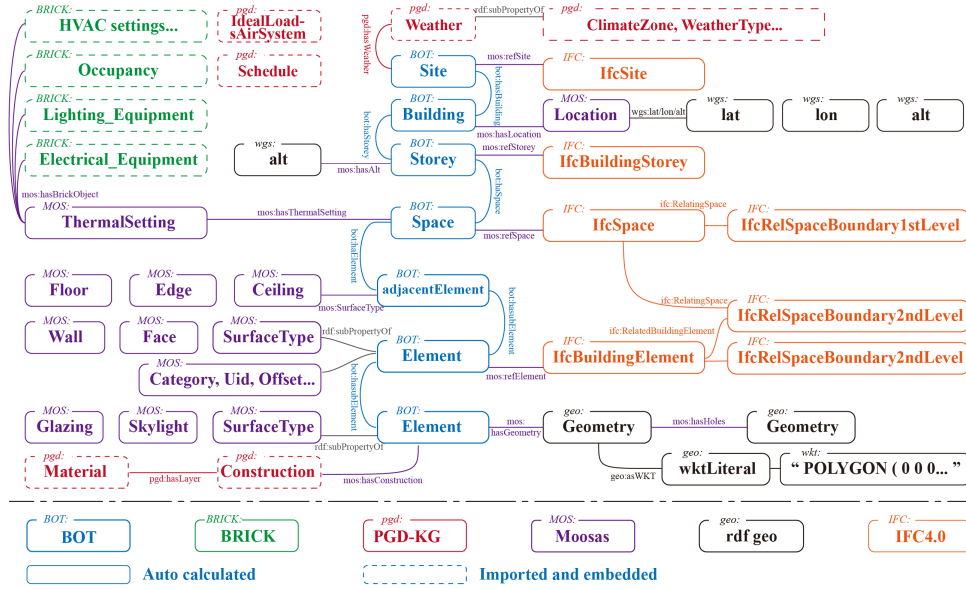


Figure 6: Ontology Definition

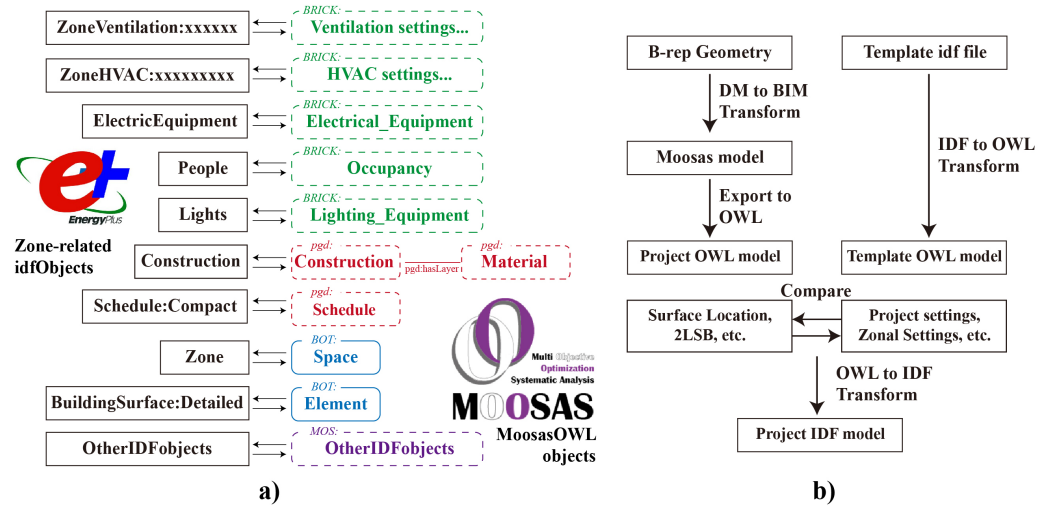


Figure 7: a) Reversible transformation between BEM and KG b) The transformation pipeline.

randomized multi-storey models with several shape parameters. A post-process script has been developed and applied to randomly create inner walls and windows to finish the thermal zoning on the parametric models following the grid axis of the building. The space volume would be maintained during the generation, which can be used to restore the space topology as well as build the energy model by Honeybee-grasshopper. Therefore, the dataset 1 is a completed auto-generated dataset with *.obj, ground truth *.owl, and ground truth *.idf for each case.

The sketch models (dataset 2) are sourced from architecture students and were specifically intended to emulate the characteristics of models produced during the early design stages. Accordingly, no restrictions are imposed regarding model cleansing, modeling techniques, or the specific design software utilized (provided an .obj file export was possible). To further challenge the module's robustness, several redundant or complex elements were intentionally introduced into the model testing sets. These included items such as shading devices, individual stair steps, and decorative façade components. The sole modeling constraint mandate that walls be represented as single surfaces rather than as two faces defining a thickness. Consequently, this dataset can be considered representative of the diverse range of model inputs encountered in practical scenarios.

The real-building models (dataset 3) are collected from important green building design cases with relatively more complex spaces and geometries. The buildings were selected according to their complexity and shapes: Oblique and Curve shape contains non-orthogonal walls and faces creating small deviation and creak; Complex floor arrangement includes high space cross multiple storeys; High-rise Oblique shape have numeric faces and spaces requires high effort on calculation; and the Complex decorated building includes numeric redundant shading and decorating elements disturbing the space and face identification. All buildings are carefully modelled with their shape, storey, and façade. Especially, considering the applications in performance analysis, the connectivity between rooms with inner walls, doors and windows are restored. This dataset is included to validate the robustness of the framework's application on real construction and design workflow.

2.3.1. Topology accuracy

The topology represented in the OWL models is validated using Dataset 1. A Grasshopper script is developed to reconstruct the space–face topology by extruding the restored space volumes. From the OWL models, a Network

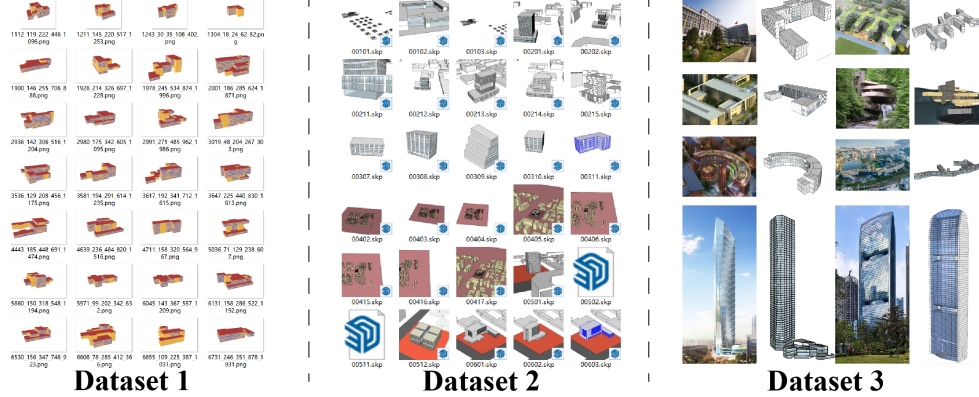


Figure 8: The three datasets used in the validation

Graph (NG) is then generated, in which construction elements (walls, floors, glazing, skylights, etc.) and spaces serve as nodes, while space–face connections and wall–window relationships are represented as edges (Fig. 5). Four evaluation metrics are designed and computed based on this graph structure.

Direct coupling between the generated graph and the ground-truth graph cannot be fully recovered during the design-model–to–BIM transformation, because the B-rep model retains only face-boundary information and excludes explicit semantic or topological labels. To address this, the ISOrank graph-alignment algorithm is employed to evaluate the correspondence between the two graphs. ISOrank computes a node-to-node Similarity score (S^{ab}), which quantifies the structural alignment between the generated graph and the ground-truth topology.

$$S_0^{ab} = \begin{cases} \min\left(\frac{D(a,b)}{0.5}, 1\right) \times \min\left(\frac{Ar_a}{Ar_b}, 1\right) & \forall \text{Type}_a = \text{Type}_b \\ 0.0 & \forall \text{Type}_a \neq \text{Type}_b \end{cases} \quad (1)$$

$$S_i^{ab} = \frac{S_{i-1}^{ab}}{N_{g_a} \cdot N_{g_b}} \cdot \sum_{p \in g_a} \sum_{q \in g_b} [(1 - \alpha) + \alpha \cdot S_{i-1}^{pq}] \quad (2)$$

$$N_{g_a} = \sum_{g_a} n, \quad N_{g_b} = \sum_{g_b} n \quad (3)$$

Here S_0^{ab} is the initial Similarity on a specific node twin (a, b) , one from the generated graph and the other from the ground truth graph; S_i^{ab} is the Similarity in the iteration i ; $D(a, b)$ is the spatial distance between a, b ; Ar

is the spaces or faces' area of the node; N_{G_a} is the total number of nodes in the graph; and α is the control parameters for better conversion on the Similarity. The nodes could therefore be coupling by iterating the similarity matrix on all nodes on the two graphs.

Besides, a metric $sN(g_1, g_2)$ indicating the total Similarity on the graphs' nodes is introduced by (4):

$$s_N(g_a, g_b) = \sum_{n \in g_a} \max_{n' \in g_b} \left\{ s^{(n, n')} \right\} / N_{g_a} \quad (4)$$

To further illustrating the accuracy on space recognition, the Similarities on all space nodes is calculated by (5): (n_s refers to the space nodes)

$$s_A(g_a, g_b) = \frac{\sum_{n_s \in g_a} (Ar_{n_s} \cdot \max_{n'_s \in g_b} \{S^{n_s, n'_s}\})}{\sum_{n_s \in g_a} Ar_{n_s}} \quad (5)$$

Thirdly, a traditional metric to illustrate the deviation during the generation is introduced [30]. The Graph Edit Distance (GED) representing how many times we need to edit the graph G_a into G_b by adding, removing, or editing a node or edge. And the negative GED (7) is a standardized metric representing the accuracy:

$$GED(g_a, g_b) = \min_{e \in \varepsilon} \sum c(e_i) \quad (6)$$

$$nGED(g_a, g_b) = 1 - \frac{GED(g_a, g_b)}{\sum n + \sum e} \quad (7)$$

Finally, a simple metric representing the calculation efficiency is introduced by (8)

$$E(g_a) = \frac{T}{\sum n_s} \quad (8)$$

2.3.2. Energy model accuracy

The accuracy between the BIM and BEM is validated by the dataset 1. The same *.idf template is used in the generation of Honeybee BEM and the transformed BEM to ensure the same thermal settings. Any topology and geometric-related properties would not be preserved from the template to the transformed BEM including the external air connection or ground connection.

Both the heating and cooling energy on multiple temporal resolutions are compared by (9) and (10).

$$\text{RMSE}_m = \sqrt{\sum_t^{N_t} \frac{(E_t - \hat{E}_t)^2}{N_t}} \quad (9)$$

$$R_t^2 = 1 - \frac{\sum_{t=0}^{N_t} (E_t - \hat{E}_t)^2}{\sum_{t=0}^{N_t} (E_t - \bar{E}_t)^2} \quad (10)$$

Here the E is the accumulated distinct cooling or heating energy for different temporal resolution in kWh/m^2 . Considering the sensitive period for cooling and heating, only the energy load on cooling/heating design days are recorded (288 timesteps for each case).

2.3.3. Transformation robustness

This framework has included multiple methods to ensure the robustness including the complex cleanse module and the fuzzy matching on the element graph during the ASG process. Besides, the whole model would be checked and any problematic elements would be remodeled in the transformation BIM to BEM. To illustrate the contribution on robustness of these modules for the whole transformation process, a robustness testing on dataset 2 with different combination of strategies is processed. Three metrics (8),(11), and (12) are collected in the test:

$$sC = \frac{\sum C_{\text{success}}}{\sum C} \quad (11)$$

$$sA = \frac{\sum Ar_{ns}}{GA} \quad (12)$$

sC : the successfully transformed cases / the total cases. sA : the recognized total floor area (Ar_{ns}) / record gross floor area (GFA)

The performance of the individual cleansing methods is evaluated, followed by a comparison of four application scenarios:

Automatic transform. DM-to-BEM transformation is executed directly on raw design models without any preprocessing. Although computationally efficient for simple geometries, this workflow is not robust and frequently fails when encountering illegal or malformed faces.

Semi-automatic transform. DM-to-BEM transformation is applied to models manually cleaned by users. In practice, the Intersect Faces with Model tool in SketchUp is executed, and decorative or non-thermal elements (e.g., stairs, shading devices, columns, beams) are removed. This improves face identifiability and reduces topological ambiguity.

Enhanced automatic transform. DM-to-BEM transformation is performed on raw models that are preprocessed using the proposed cleansing module. The cleansing stage functions similarly to SketchUp’s Intersect Faces with Model, restoring geometric consistency and improving topology detection without requiring manual intervention.

Enhanced semi-automatic transform. DM-to-BEM transformation is carried out on manually processed models with all cleansing options enabled. This scenario yields the highest overall performance, combining manual simplification with automated geometric correction, and best reflects realistic workflows expected in design-stage simulation practice.

2.3.4. Workflow efficiency and robustness

This validation focuses on assessing the framework in a realistic design workflow. A SketchUp-based interface has been developed (Fig. 9), enabling users to export B-rep data, invoke the transformation pipeline, import the generated ontology model (.xml), and produce the corresponding EnergyPlus model (.idf). To improve I/O performance, the interface employs a custom stream-based format (*.geo). This integration allows the framework to be embedded within the open-access simulation platform MOOSAS (Lin et al. 2021) and extended into a complete building simulation environment (Figure 10b).

For benchmarking, the commercial software SEFAIRA [31] is evaluated using Dataset 3. Because SEFAIRA does not provide an accessible API or automated workflow, all transformations are performed manually and documented. Efficiency is assessed using the metric in Eq. 7, with processing time captured via a mouse-tracking tool. Robustness is evaluated using Eq. 11. Each case is executed multiple times to minimize the influence of manual operations and other stochastic factors.

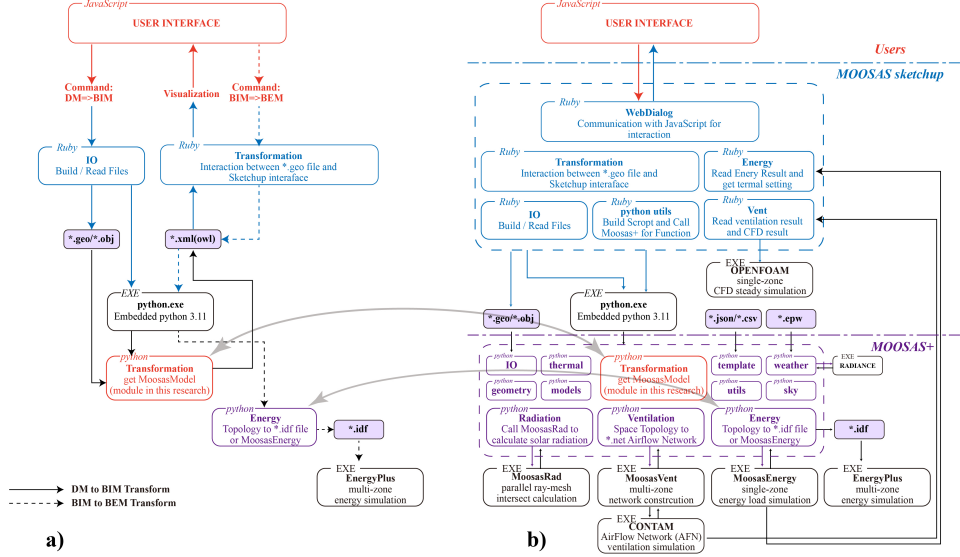


Figure 9: The embedding of the framework into Moosas+SketchUp. a) The transformation workflow inside the embedded framework. b) The whole Moosas+SketchUp Software Framework.

3. Result

3.1. Topology Accuracy from DM to BIM

Fig. 10 illustrates examples of the transformation function applied to three distinct cases from the dataset. And Fig. 11 presents the topology accuracy and computational efficiency of the three embedded ASG methods—BTG, CCR, and VFG—used to transform design models (DM) into OWL-based BIMs. Overall, the CCR method shows the strongest balance of accuracy and performance, achieving an average topological similarity of $nGED(g_a, g_b) = 0.87$ and an efficiency of $E(g_a) = 0.290$; s/room.

For element identification accuracy ($s_N(g_a, g_b)$), VFG exhibits clear advantages. Its visibility-based surface connectivity enables the highest average accuracy (0.968), outperforming CCR (0.962) and BTG (0.899). BTG struggles in irregular spaces where walls fail to connect cleanly with ground and ceiling surfaces—such as bedrooms with overhanging window ledges. These cases are reliably identified by VFG, whereas CCR partially captures them but may omit certain horizontal faces that require reattachment in later processing. As room count increases, all three methods show declining $s_N(g_a, g_b)$ performance.

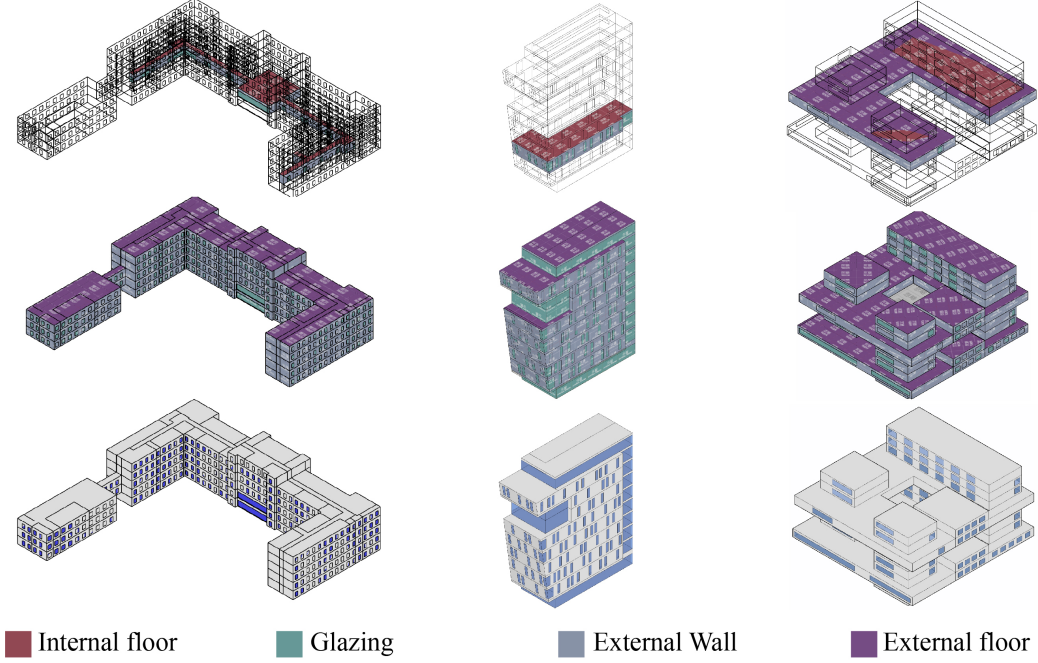


Figure 10: Transformation Visualization by the MOOSAS-SketchUp interface

Unlike s_N , the metric $s_A(g_a, g_b)$ evaluates both the number of detected space elements and their 2D boundary shapes. Here, CCR performs best, achieving an average s_A of 0.875, compared with 0.570 for VFG and 0.620 for BTG. VFG’s low s_A indicates that although it reliably locates space elements, it often fails to assemble them into coherent, closed boundaries. This limitation is correctable by tightening connectivity heuristics, but such improvements require substantially more topological computation. VFG and BTG also exhibit instability in s_A across models, especially those with only a few thermal zones.

Topological similarity, captured by $nGED(g_a, g_b)$, provides the most holistic indicator of graph-level correctness—a critical factor for downstream KG-based BEM generation. CCR again performs best (0.871), followed by VFG (0.753) and BTG (0.710). The variability in VFG stems from its stochastic ray-generation process. CCR’s performance also degrades with increased model complexity, reducing both s_A and $nGED$.

CCR further delivers the highest computational efficiency. The metric $E(g_a)$ incorporates cleansing, post-processing, and 2LSB extraction (Table

3). BTG exhibits the highest computational cost because it must evaluate full face–face connectivity for both vertical and horizontal surfaces (Fig. 4), then reconstruct wall loops—operations involving repeated Boolean calculations. BTG also inserts air-wall elements when boundaries are incomplete, increasing adjacency-solving overhead relative to CCR and VFG. In VFG, robustness improves with more rays, but this causes an exponential increase in ray–face intersection checks, making VFG substantially less efficient.

3.2. Energy Model Accuracy on BEM

Fig. 12 presents the energy-simulation accuracy. For typical usage scenarios, the full DM-to-BEM workflow using the CCR-based 1LSB method is evaluated, meaning that topology errors introduced during DM→BIM propagate into the BIM→BEM stage.

The robustness of template-setting embedding is reflected in the lighting and appliance results, which show near-zero RMSE and $R^2 \approx 1.0$ (in which

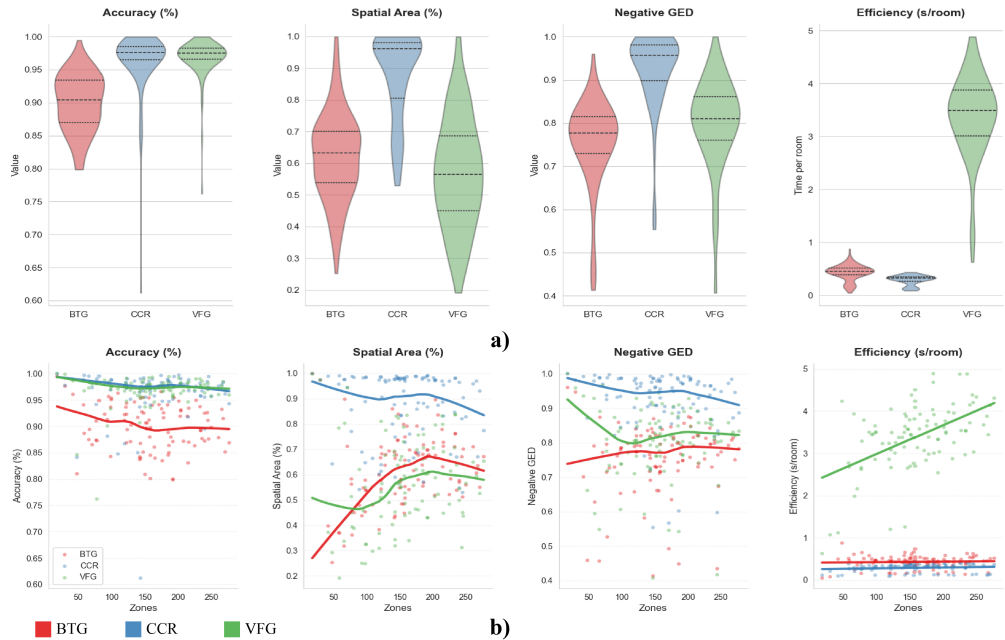


Figure 11: KG Topology validation result on datasets 1. a) Distribution of the metric on the three methods b) performance changes with the number of zones on the testing cases. Locally Weighted Scatterplot Smoothing (LOWESS) method is used to construct the fitting lines.

Table 3: Detail composition of the calculation duration for the three methods on datasets 1.

s/room	Total	I/O	Face Class.	Cleansing	1LSB	Space Pack.	2LSB
BTG	0.433	0.001	0.139	0.010	0.088	0.169	0.027
	0.23%	31.98%	31.98%	2.20%	20.25%	39.01%	6.33%
CCR	0.290	0.001	0.138	0.010	0.012	0.104	0.025
	0.35%	47.67%	47.67%	3.37%	4.14%	35.87%	8.60%
VFG	3.375	0.001	0.138	0.010	3.103	0.099	0.024
	0.03%	4.32%	4.32%	0.30%	91.71%	2.92%	0.70%

$RMSE < 10^{-12}$, kWh/m^2 , attributable to EnergyPlus numerical noise). Heating and cooling loads exhibit small deviations from the ground-truth Honeybee *.idf models, achieving monthly R^2 of 0.946 and 0.987 with RMSE of 0.51 and 0.50 kWh/m^2 . The high R^2 reveals two advantages in this module. Firstly, the validation here strictly measures the geometric fidelity passed to EnergyPlus, which means this module have high geometric fidelity in the transformation, although a standardization was implemented during the BIM→BEM stage; Secondly, the thermal settings are populated via the same IDF template to the ground truth, which means this module also have well settings fidelity.

Except for the accumulated error from topology, remaining discrepancies arise from two sources: (1) Ground-connection inconsistencies. Ground-floor detection differs between Ladybug tools and this framework: all lowest-level floor planes are treated as ground surfaces here, due to current data-structure limitations. (2) Face standardization. To ensure robustness, all faces are reconstructed from their 2D projections before *.idf generation, slightly altering geometries and introducing minor simulation deviations.

Table 4: Summary of the metric on $sN(g_a, g_b)$, $sA(g_a, g_b)$, $nGED(g_a, g_b)$ for CCR method on datasets 1.

	min	0.1	0.2	0.3	0.5	0.7	0.9	max
sN	0.612	0.939	0.957	0.967	0.975	0.983	0.991	1.000
sA	0.530	0.652	0.754	0.831	0.957	0.977	0.987	0.999
nGED	0.001	0.674	0.858	0.897	0.948	0.977	0.988	1.000

3.3. Transformation Robustness from DM to BEM

This validation assesses the robustness of the framework in early-design scenarios. Key performance metrics—robustness s_C , spatial accuracy s_A , and processing time $E(g_a)$ —are summarized in Fig. 13. Across all cleansing configurations, the cleansing module consistently improves both accuracy and robustness. Full automatic cleansing increases average robustness from 89% to 100% and spatial accuracy from 71.9% to 81.4%. It also improves efficiency by reducing problematic geometries encountered during topology generation.

A subset of 100 models from the 570-model dataset—characterized by complex forms, internal partitions, and interfering elements such as structural members and shading devices—was manually cleaned in SketchUp for comparison across four workflows.

Automatic transform, which skips all cleansing or remodeling and preserves B-rep geometry exactly, is suitable for applications requiring strict geometric fidelity. Although highly dependent on input quality, it still achieves a 95% success rate and an average s_A of 73.4%.

Semi-automatic transform, combining SketchUp’s intersection tools with manual removal of non-spatial elements, substantially improves performance, failing only in two cases and raising s_A to 81.5%.

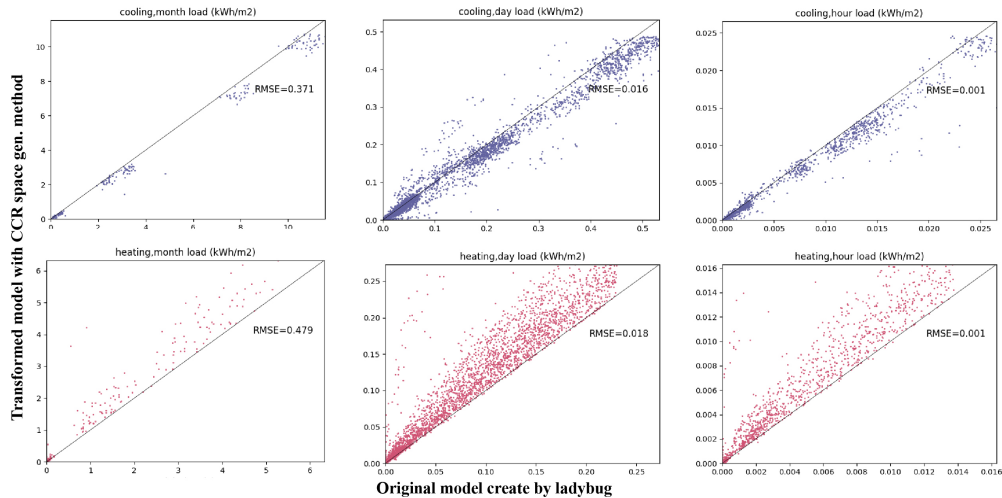


Figure 12: Energy simulation accuracy for the whole transformation from DM to BEM tested on datasets 1.

Enhanced automatic transform ensures full robustness and avoids severe errors but does not reach the same s_A as semi-automatic processing; however, it offers modest efficiency gains.

When both manual and automatic cleansing are applied, the enhanced semi-automatic workflow achieves an average s_A of 82% with no failures. It suggests that the automatic cleansing may be safely skipped in some cases to accelerate computation without significant loss of topological accuracy.

3.4. Workflow efficiency and robustness

To evaluate the framework in real-world applications, it was embedded in MOOSAS and compared with the commercial software SEFAIRA on the SketchUp platform. As SEFAIRA is closed-source, face classification and energy analysis were executed and recorded manually, using accessible metrics s_A and $E(g)$ (with GFA measured directly from the model)(Table. 5). SEFAIRA does not provide spatial topology results; its interface only displays automatically classified face tags and performs BEM transformation and analysis as a single process. In this evaluation, face classification—including partial cleansing—is decoupled from the remainder of transformation in the framework, while MOOSAS Energy is used to assess the complete DM-to-BPS workflow. Besides, to exclude the I/O issues and focus on the main efficiency and accuracy, before the start of transformation, the *.geo files

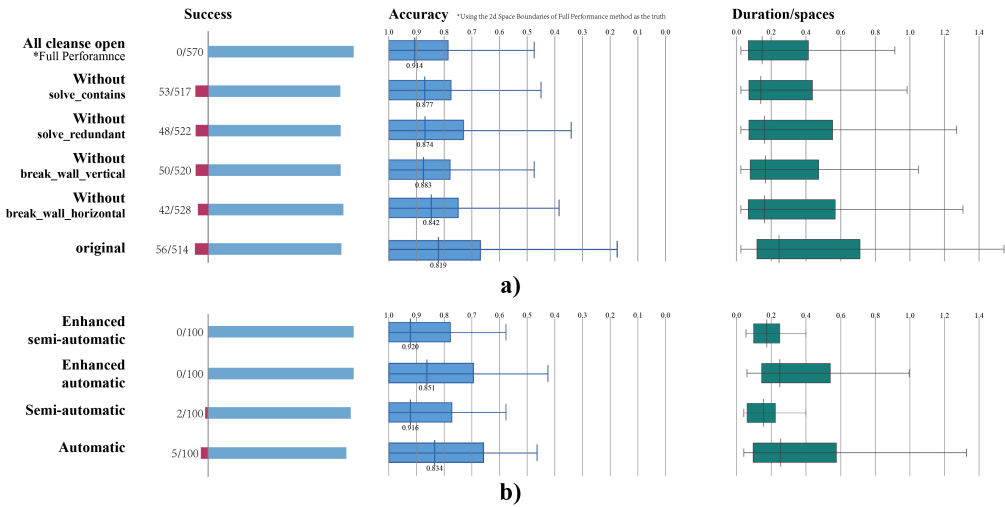


Figure 13: Comparison between cleanse method tested on datasets 2. a) The implementation on four cleanse methods. b) Combination with the manual cleanse in SketchUp.

were exported from sketchUp models which will directly run the SEFAIRA transformation.

SEFAIRA exhibits more stable and efficient face classification in simple cases, but its performance declines for high-rise buildings (cases 12–14) due to delays from complex cleansing. In buildings with intricate spatial arrangements (cases 6–11), SEFAIRA shows poor robustness and fails to complete the full transformation. Notably, in case 15 (Fallingwater Apartment), which contains numerous shading, decorative, and structural elements, GFA deviation reaches 638%, indicating failure to filter redundant items.

In contrast, the proposed framework maintains high stability across all cases, with a maximum s_A error of 22%. Case 5, a curved building, exhibits $s_A = 0.78$, highlighting limitations in handling irregular geometries. For case 15, GFA is overestimated because massive walls are misidentified as spaces, suggesting the need for additional filtering of invalid spaces in future versions.

4. Discussion

The primary contribution of this work lies in enabling explicit graph-based representations from flexible, unstructured design models, allowing AI systems to directly interpret spatial configurations, element relationships, and performance-relevant attributes in early design. By transforming boundary-representation geometry into topology-aware Knowledge Graph (KG) and Network Graph (NG) structures, the framework overcomes a key barrier that previously limited AI reasoning and control over automated design and analysis pipelines.

The inclusion of multiple analytical outputs—energy, ventilation, and daylighting—broadens AI-driven applications by linking graph-based representations to diverse performance domains, enabling evaluation, comparison, and multi-objective optimization within a unified, automated workflow. Implemented in the MOOSAS+ simulation environment [27], the framework integrates with existing BPAM modules and supports EnergyPlus, RADIANCE, CONTAM, and OpenFOAM, transforming a single B-rep model into multiple analysis-ready representations while preserving design flexibility.

Compared to conventional workflows (Table 6), the pipeline reduces manual remodeling and latency and provides a unified information substrate for AI. Coupled with grey-box or surrogate models such as Graph Neural

Table 5: Compare the application on real building to commercial software SEFAIRA on datasets 3.

case	GFA (m^2)	This Study			SEFAIRA		
		E(g) (s)		sA	E(g) (s)		sA
		Classify	Analyze		Classify	Analyze	
1	18617.05	8.06	12.72	1.00	2.54	107.11	1.21
2	390.80	0.61	2.00	1.00	2.70	39.74	2.15
3	83948.63	16.57	104.86	0.82	2.89	122.39	1.32
4	23247.22	2.96	25.16	0.86	2.55	73.03	1.26
5	4793.64	1.13	5.44	0.78	2.13	36.32	1.37
6	8128.79	6.34	6.23	1.02	N/A	N/A	N/A
7	447471.00	1.97	1.46	1.01	N/A	N/A	N/A
8	156403.00	2.73	7.38	0.96	2.75	122.83	1.79
9	261670.16	4.60	22.07	0.90	2.92	167.50	3.50
10	127673.28	18.78	201.59	1.00	N/A	N/A	N/A
11	25745.77	0.80	6.18	0.99	N/A	N/A	N/A
12	447206.65	18.16	64.77	1.00	N/A	N/A	N/A
13	196788.64	13.06	51.95	1.12	N/A	N/A	N/A
14	170383.69	11.98	40.21	1.03	2.28	212.71	0.93
15	395.69	3.27	5.88	1.20	2.58	252.84	7.38

Networks (GNNs) or KG-enhanced LLMs, it enables fully automated, accelerated simulation–optimization loops and interactive performance-driven design.

As the first open-access, fully automated, and reversible DM–BIM–BEM framework, it demonstrates superior robustness and spatial accuracy, particularly for complex geometries. With MOOSAS Energy compatibility, it achieves analysis times of 0.01s per zone and 0.29s for full DM-to-BEM transformation, supporting high-frequency evaluation, real-time feedback, and AI-driven optimization, providing a practical infrastructure for intelligent construction workflows.

Table 6: comparison on the level of automation to existing software providing the whole DM to BIM workflow

	This study	SEFAIRA	Cove.tools	Ladybug
	Open-access	Closed	Closed	Open-access
Cleansing	Auto	Semi-Auto	Semi-Auto	Manual
Classification	Auto	Auto	Manual	Auto
ASG (1LSB)	Auto	Auto	Auto	Manual
Topology (2LSB)	Auto	Auto	Auto	Semi-Auto
Thermal Embedding	Auto	Auto	Auto	Auto
BPAM Generation	Auto	Auto	Auto	Auto

4.1. Limitation

Despite its robustness and automation, the framework exhibits several limitations. The cleansing module emphasizes transformation robustness over accuracy, yielding smaller gains in s_A than semi-automatic workflows, which may constrain fully automated applications such as building performance optimization or AI-based preprocessing (GNN/KG-LLM), though manual correction is straightforward. Efficiency is also limited, with face classification and space construction consuming on average 83% of processing time, highlighting a key area for optimization. Geometric modifications during cleansing can introduce errors, including self-intersections from CSG operations (by pygeos), requiring future remediation. Finally, the framework does not yet implement automated subdivision of contiguous thermal zones or elongated spaces (e.g., corridors), which is essential for accurately capturing variable thermal loads and generating robust building energy models.

Future development will target enhanced automatic cleansing, improved efficiency, geometric validation, and automated thermal zoning to support fully end-to-end BPS workflows.

4.2. Applications

This framework uniquely converts unstructured boundary-representation (B-rep) design geometry into explicit graph representations—Knowledge Graphs (KGs) and Network Graphs (NGs)—that encode spaces, elements and their topological relations. By producing AI-ready, topology-explicit models from early conceptual geometry (Fig. 14), the framework unlocks a spectrum of automated and learning-based applications:

Graph-based performance prediction and surrogate modeling. GNNs can consume NG/KG outputs to predict thermal, daylighting or ventilation performance at room and building scales, enabling ultra-fast surrogate evaluation in optimization loops.

Knowledge-augmented LLM workflows. KG-RAG pipelines let LLMs answer design queries, generate constraint-aware suggestions, or produce natural-language explanations grounded in an explicit building graph (improving interpretability and traceability).

Automated multi-objective optimization and control. Combined with grey-box models or reinforcement learning agents, the pipeline supports automated, performance-driven design exploration (e.g., trade-offs among energy, daylight, and ventilation) directly from conceptual sketches.

Transfer learning and dataset augmentation. By converting legacy and student sketch datasets (B-rep) into unified graph formats, the framework greatly expands training corpora for data-driven methods and facilitates domain transfer between projects and scales.

Urban and multi-method workflows. Graph outputs enable neighborhood-scale analytics (UBEM) and seamless coupling between mesh-based (CFD, RADIANCE) and topology-based (AFN, EnergyPlus) simulations for integrated, multi-physics studies.

To support these uses, the framework supplies modular transformation tools and interchange formats: (1) *.obj to *.geo cleansing and fast I/O; (2) .geo / MoosasModel and KG (.rdf, .owl) with optional 2LSB/IFC4 semantics; and (3) MoosasModel and NG (.xml, *.json) with pruning for ML efficiency. These modules are reversible and scriptable (APIs provided), enabling automated pipelines for training, inference, interactive feedback, and continuous integration with simulation engines and ML toolchains.

By bridging flexible design geometry and graph-centric AI representations, the framework provides an infrastructure layer that amplifies the reach of graph-based and language-enabled intelligence across early design, optimization, and construction informatics—facilitating reproducible, scalable, and explainable automation.

5. Conclusion

This paper presents a novel and robust geometry-transformation framework that bridges unstructured B-rep Design Models (DM), knowledge-graph-based Building Information Models (BIM), and EnergyPlus Building Energy Models (BEMs). The framework integrates six cleansing methods and three 1LSB Auto Space Generation (ASG) approaches, and systematically evaluates their combined performance.

Validation across three DM datasets demonstrates that the framework achieves a 100% processing success rate, maintains high robustness with all cleansing modules enabled, and produces BIM KGs with an average space-related topology accuracy of 0.871 (nGED). The framework further produces analytical BEMs with sufficient fidelity to support performance-informed AI applications.

By enabling fully automatic transformations from DM to BIM and BEM, the framework extends NG- and KG-based BIM techniques and AI intervention to unstructured design models, unlocking a range of novel applications. This facilitates graph neural network (GNN)-based performance prediction, knowledge-graph-enhanced large language model (KG-LLM) reasoning, BIM-based optimization directly from conceptual sketches, and scalable urban-level analysis workflows.

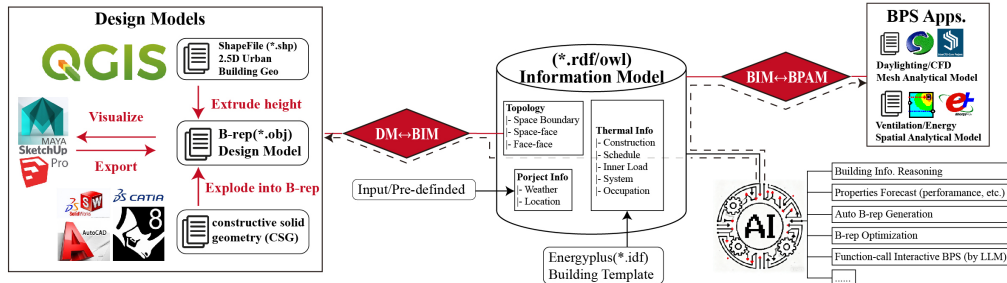


Figure 14: Potential applications with this framework.

Future work will focus on improving computational efficiency, mitigating geometric artifacts, and enhancing thermal and functional zoning, further strengthening the framework as an AI infrastructure for early-stage design intelligence.

6. Data Availability

The Moosas package and testing code is available through:

<https://github.com/KLEGKB/moosas>

A reproducible example is available via Code Ocean capsule:

<https://doi.org/10.24433/C0.2302305.v2>

The validation model dataset and code are partly accessible: dataset 1 and 3, the script for automatic model generation, and the restoration of space topology in grasshopper, and the script for automatic energy modelling on the parametric model dataset 1. Researchers can fully reproduce or generate more parametric model directly with the script. The description and models could be found via:

<https://doi.org/10.6084/m9.figshare.30693461.v1>

7. Acknowledgments

The study was supported by the National Natural Science Foundation of China (Grant No.52425801, 52394223 and 52130803).

References

- [1] P. Warren, Bringing Simulation to Application, Tech. Rep. A30-TSR-09-2002, FaberMaunsell Ltd, St Albans, United Kingdom, backup Publisher: International Energy Agency Energy Conservation in Buildings and Community Systems Programme (IEA-ECBCS) (2002). URL https://annex53.iea-ebc.org/Data/publications/EBC_Annex_30_tsr_final.pdf
- [2] P. B. Purup, S. Petersen, Requirement analysis for building performance simulation tools conformed to fit design practice, Automation in Construction 116 (2020) 103226. doi:10.1016/j.autcon.2020.103226. URL <https://linkinghub.elsevier.com/retrieve/pii/S0926580519314438>

- [3] W. Ma, H. Chen, G. Zhang, Y.-C. Chou, J. Chen, C. M. de Melo, A. Yuille, 3DSRBench: A comprehensive 3d spatial reasoning benchmark, in: Proceedings of the IEEE/CVF International Conference on Computer Vision (ICCV), 2025, pp. 6924–6933, open Access version provided by Computer Vision Foundation; final published version available on IEEE Xplore. doi:10.1109/ICCV.2025.00692.
URL https://www.openaccess.thecvf.com/content/ICCV2025/papers/Ma_3DSRBench_A_Comprehensive_3D_Spatial_Reasoning_Benchmark_ICCV_2025_paper.pdf
- [4] S. Ji, S. Pan, E. Cambria, P. Marttinen, P. S. Yu, A Survey on Knowledge Graphs: Representation, Acquisition, and Applications, *IEEE Transactions on Neural Networks and Learning Systems* 33 (2) (2022) 494–514. doi:10.1109/TNNLS.2021.3070843.
URL <https://ieeexplore.ieee.org/document/9416312/>
- [5] M. Li, Z. Wang, BuildingGPT: Query building semantic data using large language models and vector-graph retrieval-augmented generation, *Building and Environment* 287 (2026) 113855. doi:10.1016/j.buildenv.2025.113855.
URL <https://linkinghub.elsevier.com/retrieve/pii/S0360132325013253>
- [6] Z. Wu, M. Li, W. Liu, J. C. P. Cheng, Z. Wang, H. H. L. Kwok, C. Huang, F. Hou, Developing surrogate models for the early-stage design of residential blocks using graph neural networks, *Building Simulation* (Jan. 2025). doi:10.1007/s12273-025-1237-7.
URL <https://link.springer.com/10.1007/s12273-025-1237-7>
- [7] M. H. Rasmussen, P. Pauwels, M. Lefrançois, G. F. Schneider, Building Topology Ontology (BOT), Draft Community Group Report, World Wide Web Consortium Linked Building Data Community Group (W3C LBD-CG) (2025).
URL <https://w3c-lbd-cg.github.io/bot/>
- [8] Brick Schema Community, Brick: A Uniform Metadata Schema for Buildings (2025).
URL <https://brickschema.org/>

- [9] buildingSMART International, ifcOWL (2025).
 URL <https://technical.buildingsmart.org/standards/ifc/ifc-formats/ifcowl/>
- [10] buildingSMART, IfcRelSpaceBoundary1stLevel (2023).
 URL <https://standards.buildingsmart.org/IFC/RELEASE/IFC4/ADD2a/TC1/HTML/schema/ifcproductextension/lexical/ifcrelspaceboundary1stlevel.htm>
- [11] buildingSMART, IfcRelSpaceBoundary2ndLevel (2023).
 URL <https://standards.buildingsmart.org/IFC/RELEASE/IFC4/ADD2a/TC1/HTML/schema/ifcproductextension/lexical/ifcrelspaceboundary2ndlevel.htm>
- [12] S. Li, Z. Jiang, Z. Xu, BIM-Based Model Checking: A Scientometric Analysis and Critical Review, *Applied Sciences* 15 (1) (2024) 49. doi:10.3390/app15010049.
 URL <https://www.mdpi.com/2076-3417/15/1/49>
- [13] Z. Wu, Z. Wang, J. C. Cheng, H. H. Kwok, A knowledge-informed optimization framework for performance-based generative design of sustainable buildings, *Applied Energy* 367 (2024) 123318. doi:10.1016/j.apenergy.2024.123318.
 URL <https://linkinghub.elsevier.com/retrieve/pii/S0306261924007013>
- [14] C. M. Rose, V. Bazjanac, An algorithm to generate space boundaries for building energy simulation, *Engineering with Computers* 31 (2) (2015) 271–280. doi:10.1007/s00366-013-0347-5.
 URL <http://link.springer.com/10.1007/s00366-013-0347-5>
- [15] D. Ladenhauf, K. Battisti, R. Berndt, E. Eggeling, D. W. Fellner, M. Gratzl-Michlmair, T. Ullrich, Computational geometry in the context of building information modeling, *Energy and Buildings* 115 (2016) 78–84. doi:10.1016/j.enbuild.2015.02.056.
 URL <https://linkinghub.elsevier.com/retrieve/pii/S0378778815001802>
- [16] H. Ying, S. Lee, Generating second-level space boundaries from large-scale IFC-compliant building information models using multiple

geometry representations, *Automation in Construction* 126 (2021) 103659. doi:10.1016/j.autcon.2021.103659.
 URL <https://linkinghub.elsevier.com/retrieve/pii/S0926580521001102>

[17] H. Ying, S. Lee, A rule-based system to automatically validate IFC second-level space boundaries for building energy analysis, *Automation in Construction* 127 (2021) 103724. doi:10.1016/j.autcon.2021.103724.
 URL <https://linkinghub.elsevier.com/retrieve/pii/S0926580521001758>

[18] H. Chen, Z. Li, X. Wang, B. Lin, A graph- and feature-based building space recognition algorithm for performance simulation in the early design stage, *Building Simulation* 11 (2) (2018) 281–292. doi:10.1007/s12273-017-0412-x.
 URL <https://doi.org/10.1007/s12273-017-0412-x>

[19] N. L Jones, C. J Mccrone, B. J Walter, K. B Pratt, D. P Greenberg, Automated Translation And Thermal Zoning Of Digital Building Models For Energy Analysis, 2013. doi:10.26868/25222708.2013.1027.
 URL <https://publications.ibpsa.org/conference/paper/?id=bs2013Ѓ>

[20] J. Xiao, H. Zhou, S. Yang, D. Zhang, B. Lin, A CAD-BEM geometry transformation method for face-based primary geometric input based on closed contour recognition, *Building Simulation* (Dec. 2023). doi:10.1007/s12273-023-1081-6.
 URL <https://link.springer.com/10.1007/s12273-023-1081-6>

[21] M. Wang, G. N. Lolis, D. Mavrokapis, K. Katsigarakis, I. Korolija, D. Rovas, A knowledge graph-based framework to automate the generation of building energy models using geometric relation checking and HVAC topology establishment, *Energy and Buildings* 315 (2024) 115035. doi:10.1016/j.enbuild.2024.115035.
 URL <https://www.sciencedirect.com/science/article/pii/S0378778824011514>

[22] P. Iliadis, E. Bellos, R. Rotas, A. Kitsopoulou, N. Ziozas, N. Nikolopoulos, Comprehensive framework for dynamic energy assessment of building systems using IFC graphs and Modelica, *Jour-*

nal of Building Performance Simulation 18 (4) (2025) 478–499. doi:10.1080/19401493.2024.2449375.

URL <https://www.tandfonline.com/doi/full/10.1080/19401493.2024.2449375>

[23] H. Sayegh, G. N. Lolis, M. Bouquerel, T. Duforestel, K. Katsigarakis, D. Rovas, Automatic Modelica BEM generation from IFC BIM, in: Proceedings of the 2024 IEEE International Workshop on Metrology for Living Environment (MetroLivEnv), IEEE, Chania, Greece, 2024. doi:10.1109/MetroLivEnv60384.2024.10615614.

URL <https://doi.org/10.1109/MetroLivEnv60384.2024.10615614>

[24] D. Jansen, P. Mehrfeld, D. Müller, E. Fichter, V. Richter, A. Barz, J. Brunkhorst, M. Dahncke, P. Jahangiri, C. Warnecke, P. Mehrfeld, J. Frisch, C. Van Treeck, B. L. Bruno Lüdemann, BIM2SIM - Development of semi-automated methods for the generation of simulation models using Building Information Modeling, 2021. doi:10.26868/25222708.2021.30228.

URL https://publications.ibpsa.org/conference/paper/?id=bs2021_30228

[25] A. Andriamamonjy, D. Saelens, R. Klein, An automated IFC-based workflow for building energy performance simulation with Modelica, Automation in Construction 91 (2018) 166–181. doi:10.1016/j.autcon.2018.03.019.

URL <https://linkinghub.elsevier.com/retrieve/pii/S0926580517308282>

[26] S. Pinheiro, R. Wimmer, J. O. Donnell, S. Muhic, F. N. [Author 5], F. N. [Author 6], F. N. [Author 7], F. N. [Author 8], MVD based information exchange between BIM and building energy performance simulation, Automation in Construction 90 (2018) 91–103. doi:10.1016/j.autcon.2018.02.009.

URL <https://doi.org/10.1016/j.autcon.2018.02.009>

[27] B. Lin, H. Chen, Q. Yu, X. Zhou, S. Lv, Q. He, Z. Li, MOOSAS – A systematic solution for multiple objective building performance optimization in the early design stage, Building and Environment 200 (2021) 107929. doi:10.1016/j.buildenv.2021.107929.

URL <https://linkinghub.elsevier.com/retrieve/pii/S0360132321003334>

- [28] World Wide Web Consortium (W3C), W3C Geo Vocabulary (2024).
URL <https://www.w3.org/2003/01/geo/>
- [29] L. Wang, P. Janssen, G. ji, SSIEA: a hybrid evolutionary algorithm for supporting conceptual architectural design, *Artificial intelligence for engineering design analysis and manufacturing* 34 (2020) 1–19. doi:10.1017/S0890060420000281.
- [30] Y. Liu, H. Huang, G. Gao, Z. Ke, S. Li, M. Gu, Dataset and benchmark for as-built BIM reconstruction from real-world point cloud, *Automation in Construction* 173 (2025) 106096. doi:10.1016/j.autcon.2025.106096.
URL <https://linkinghub.elsevier.com/retrieve/pii/S0926580525001360>
- [31] Sefaira, Sefaira (2023).
URL <https://www.sketchup.com/products/sefaira>